Efficient parameterization of adsorbate–adsorbate interactions on metal surfaces

Surface Science 754 (2025) 122678

Contents lists available at ScienceDirect

Surface Science

journal homepage: www.elsevier.com/locate/susc

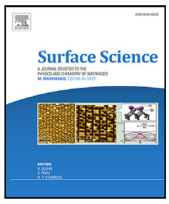

Efficient parameterization of adsorbate–adsorbate interactions on metal surfaces

Willem Vanmoerkerke *, Rasmus Svensson *, Henrik Grönbeck *

Department of Physics and Competence Centre for Catalysis, Chalmers University of Technology, Göteborg, SE-412 96, Sweden

ARTICLE INFO

Keywords:
Adsorption
Adsorbate–adsorbate interactions
DFT calculations
Kinetic modeling

ABSTRACT

Quantitative modeling of surface reactions relies on accurate potential energy surfaces that include adsorbate–adsorbate interactions. Using density functional theory calculations we introduce an efficient procedure to parameterize adsorbate–adsorbate interactions and present results for interactions between O_2, O, OH and H_2O on Pt, Ir, Rh and Pd surfaces. The targeted interactions are important when describing, for example, the electrochemical oxygen reduction reaction. However, an accurate representation of both non-directional interactions and directional hydrogen bonds remains challenging. By analyzing the dominant contributions, we find that accurate parameterizations can be constructed by separately considering surface mediated electronic interactions and pairwise hydrogen bonds. Two methods are evaluated to account for interactions beyond nearest-neighbors. Our work provides a general framework to analyze adsorbate–adsorbate interactions and present parameterizations suitable for efficient kinetic Monte Carlo simulations.

1. Introduction

First-principles based kinetic modeling of surface reactions has developed into an integrated part of heterogeneous catalysis research [1]. Kinetic models have the possibility to provide atomistic-level understanding of governing reaction mechanisms [2,3] and assist catalyst design [4]. The potential energy surface in first-principles based kinetic modeling is commonly obtained using Density Functional Theory (DFT) calculations and the reaction kinetics is modeled using either mean-field or kinetic Monte Carlo (kMC) simulations [5]. The reaction kinetics is in the mean-field approach described by coverages with the fundamental assumption that the adsorbates are randomly distributed and completely mixed. The kinetic Monte Carlo approaches are instead based on transitions between states with explicit adsorbate distributions. The success of first-principles based kinetic models relies on an accurate potential energy surface. A general challenge is that the stability of surface species and barriers for surface reactions depend sensitively on the local environment of the reactants, which is determined by the surface sites and the interaction between adsorbates.

It is well-known that adsorbate–adsorbate interactions (AAI) can affect the stability of adsorbates and the kinetics of surface reactions significantly [6,7]. AAI models for first-principles based kinetic models are typically developed by calculations of adsorbates structures with different surface cells and coverages. For mean-field models, the adsorption energies are obtained as a function of the coverages and parameterizations may use linear, exponential or polynomial functional forms [8,9]. The AAIs are in kinetic Monte Carlo simulations instead based on cluster expansion models with explicit nearest neighbor and, in some cases, next-nearest neighbor interactions [10,11]. The inclusion of AAI in kMC models can lead to non-trivial adsorbate ordering, which may affect the catalytic performance [12–14]. The accuracy of the applied parameterizations can be evaluated, for example, by comparisons to temperature programmed desorption and reaction experiments [15,16].

AAI models are generally developed without explicitly targeting the dominating mechanisms for the interactions. Although this approach has resulted in accurate models [17], it could be advantageous to understand the underlying mechanisms to facilitate the development of accurate models with fewer parameters. Detailed understanding could, in particular, be valuable for AAI models used in kMC simulations, where models rely on explicit nearest neighbor and next-nearest neighbor interactions [18]. The AAIs could have different origins, including (i) direct electrostatic interactions from polar adsorbates or dipoles formed between the surface and the adsorbates [19], (ii) surface mediated electronic effects, such as d-band shifts and charge redistribution effects [20], (iii) structural distortions of the surface via adsorbate-induced strain [21], and (iv) hydrogen bonds [22]. The first three interactions types are interlinked, whereas hydrogen bonding is of different character, and present only between adsorbates with hydrogen atoms and electron lone-pairs.

* Corresponding authors.
E-mail addresses: willemvm@mit.edu (W. Vanmoerkerke), rassve@chalmers.se (R. Svensson), ghj@chalmers.se (H. Grönbeck).

https://doi.org/10.1016/j.susc.2024.122678
Received 24 September 2024; Received in revised form 3 December 2024; Accepted 5 December 2024
Available online 12 December 2024

Here we use DFT calculations to develop interaction models for O, OH, H_2O, and O_2 adsorbates on Pt, Ir, Rh and Pd surfaces. The adsorbates are chosen owing to their importance in a range of electrochemical applications, where the oxygen reduction reaction in proton exchange membrane fuel cells is but one example [23]. The AAI models are developed based on an analysis of the dominant interaction mechanisms. We find that accurate parameterizations can be obtained by considering surface mediated electronic interactions and pair-wise hydrogen bonds. The obtained parameterizations can be efficiently implemented in kMC simulations.

2. Methods

Spin-polarized density functional theory (DFT) calculations are performed using the Vienna Ab Initio Simulation Package (VASP) [24–27]. The projector-augmented wave (PAW) method is used to describe the interactions between core and valence electrons [28,29]. The considered valence electrons are: $1s^1$ (H), $2s^22p^4$ (O), $5s^14d^8$ (Rh), $5s^14d^9$ (Pd), $6s^15d^8$ (Ir) and $6s^15d^9$ (Pt).

The Perdew–Burke–Ernzerhof (PBE) functional is employed to describe exchange–correlation effects [30]. The PBE functional is augmented with the D3-correction to account for dispersion interactions [31,32]. The Kohn–Sham orbitals are expanded with plane-waves truncated at an energy cutoff of 450 eV. A Gaussian smearing with a standard deviation of 0.1 eV is applied to facilitate convergence, and the total energy is extrapolated to zero standard deviation. The convergence criterion for the electronic structure is set to a change in electronic energy and Kohn–Sham eigenvalues of less than 1×10^{-6} eV between successive iterations.

The (111), (100) and (211) surfaces are modeled using $p(3 \times 3)$ super-cells with four atomic layers. The periodic slabs are separated by 20 Å of vacuum and the bottom two layers of the slabs are fixed to the corresponding bulk positions during the structural optimization. The Brillouin zone is sampled using a Γ-centered k-point $(7 \times 7 \times 1)$ grid for Pd slabs, whereas a $(5 \times 5 \times 1)$ grid is used for Pt, Ir, and Rh slabs. Structural relaxations are performed using the conjugate gradient method until the forces on all atoms are smaller than 0.03 eV/Å. Bader analyses are used to determine the charge of adsorbates [33–36].

The change in adsorption energy (the interaction energy) for an adsorbate x_i of specie X_i on a metal surface with a specified coverage is defined according to:

$$\begin{aligned}\Delta E_{\text{ads}}^{x_i} &= \underbrace{E^{\text{cov}+x_i} - E^{\text{cov}} - E_{\text{ref}}^{X_i}}_{\text{adsorption energy on covered surface}} - \underbrace{(E^{x_i} - E^{\text{bare}} - E_{\text{ref}}^{X_i})}_{\text{adsorption energy on clean surface}} \\ &= E^{\text{cov}+x_i} + E^{\text{bare}} - E^{\text{cov}} - E^{x_i}, \end{aligned} \quad (1)$$

where $E^{\text{cov}+x_i}$ is the energy of a surface with the coverage cov, and an additional adsorbate x_i. E^{cov} is the energy of the surface with a coverage cov. $E_{\text{ref}}^{X_i}$ is the reference energy of specie X_i (*i.e.* the gas-phase energy). E^{x_i} is the energy of the surface with an isolated x_i adsorbate, and E^{bare} is the energy of a clean metal surface.

The AAIs owing to hydrogen bonds are compared to previous experiments and *ab initio* molecular dynamics simulations by performing kMC simulations of an OH/H_2O layer on a Pt(111) surface using the MonteCoffee code [11]. As the network of adsorbate configurations with hydrogen bonds are governed by directional bonds, events of surface diffusion and hydrogen-transfer reactions are augmented with rotations of adsorbed OH and H_2O. For simplicity, only six orientations of the hydrogen atoms and the lone electron pairs are allowed, where they are oriented towards a specific nearest neighbor. A hydrogen bond is only formed when the hydrogen donor points towards the acceptor and the acceptor points towards the donor. Thermodynamic consistency in the equilibration of the adsorbate configurations is maintained by describing all reverse reaction rate constants, k_r, from the forward reaction rate constant k_f as:

$$k_r = \frac{k_f}{K} \approx k_f e^{\Delta E / k_B T}, \quad (2)$$

where K is the equilibrium constant, ΔE is the reaction energy, k_B is the Boltzmann constant, and T is the temperature. The adsorbate configurations are optimized at a temperature of 300 K.

3. Results

The aim of this work is to develop a robust AAI model for O, O_2, OH, and H_2O adsorbed on metal surfaces. Using atomic oxygen as a model for oxygen containing adsorbates, we first investigate the dominating contributions to the AAI of adsorbed O. We find that surface-mediated effects dominate the interactions and develop as a second step a framework to account for AAIs based on this finding. Hydrogen bonds are thereafter shown to be directional and additive. The models for surface-mediated interactions and hydrogen bonds are combined and validated by comparisons to DFT calculations for adsorbate structures on (111), (100), and (211) surfaces of Rh, Pd, Ir and Pt.

3.1. Dominating mechanism of O–O interactions

The O–O interactions on Pt(100) are used to investigate the dominating interaction mechanisms for the oxygen containing adsorbates. O adsorbates are negatively charged by ~0.6 e and interact by direct electrostatic interactions as well as surface mediated interactions, owing to surface distortions and adsorbate-induced modifications of the electronic structure. To understand the dominating mechanism, we investigate three different configurations on Pt(100), see Fig. 1. The O atoms can be adsorbed to the same metal atom as in configurations I and II (M-connected) and configuration V (diagonal). Another possibility is configurations III and IV (side-by-side), where the O atoms are adsorbed on different surface atoms. Note that the O–O distances are approximately the same in configurations I and III.

Pt(100) offers a convenient surface to study the main contributions to the AAIs. The interaction will depend on the inter-atomic distance and charging of adsorbates if direct electrostatic interactions between the O atoms dominate. As the distance between adsorbates is the same for configurations I and III and their charges are only marginally different (Bader charges of 0.62 e and 0.61 e per O, respectively), the interaction energy should be similar if direct electrostatic interactions dominate.

The O adsorbates increase the spacing between the metal surface atoms to which they are connected and, consequently, induce local surface strain. In configuration I, the surface atom bound to both O-atoms experience forces in opposite directions giving rise to compressive strain, which is known to reduce adsorbate stability [37]. Instead, when the O atoms are placed in configuration III (side-by-side), the two adsorbates affect different surface atoms, and create effectively a tensile strain, which generally leads to enhanced stability [37]. To conclude, if surface distortions dominate the interactions, configuration I is expected to show a stronger interaction energy than does configuration III.

The O–Pt bond leads to rehybridization of the metal atoms, which affects the neighboring O–Pt bonds. This is a surface mediated electronic interaction, which, for example, is visible by adsorbate induced shifts in the metal d-band centers [20]. If this type of surface mediate electronic effects dominate the AAIs, the interaction energy is expected to be most pronounced in configurations I, II and V, as the electronic change on surface atoms with adsorbate bonds is larger than on surface atoms without adsorbate bonds.

The calculated interaction energies [Eq. (1)] of the five configurations in Fig. 1 are reported in Fig. 2. Fig. 2a shows the interactions energies as a function of the nearest neighbors and Fig. 2b as a function of the strain at the site of adsorption. The interaction energies for configurations I and II (M-connected) are clearly positive, whereas the interaction energies for configurations III and IV are slightly negative. The marked difference between the M-connected and the side-by-side configurations signals that direct electrostatic interactions do not

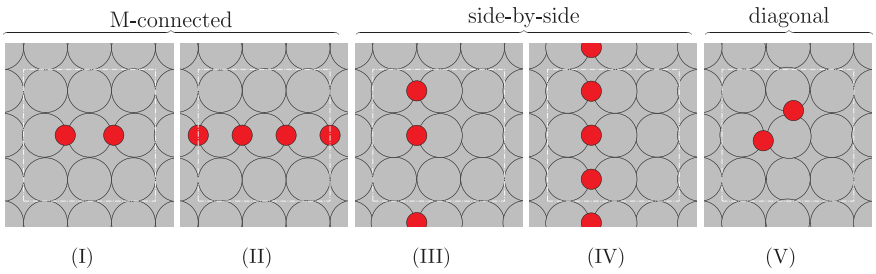

Fig. 1. O adsorbate configurations on Pt(100). The periodic cell is marked by dash-dotted white lines. Atomic color codes: gray (Pt) and red (O).

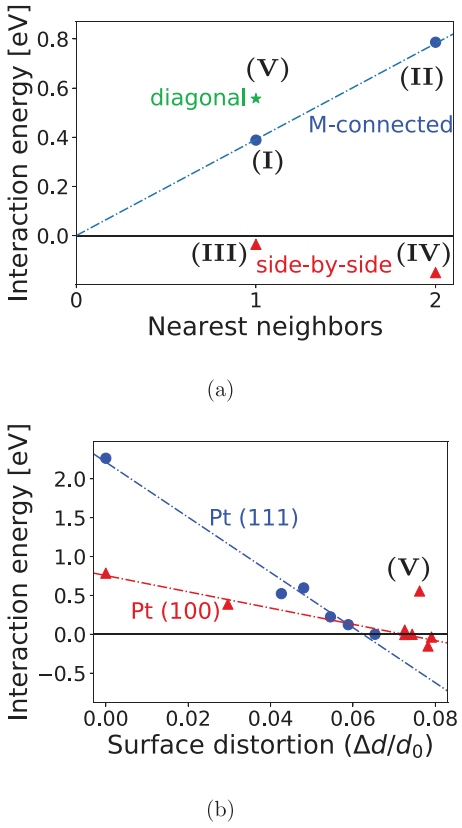

Fig. 2. (a) Interaction energy of the structures visualized in Fig. 1, as a function of the number of nearest O neighbors. The roman numerals indicate the labels of the configurations in Fig. 1. (b) Interaction energy as a function of the local surface strain, defined as the relative change of the M–M distance between the metal atoms the adsorbate is bonded to. Besides the structures in Fig. 1, structures from Table S1 are added sampling the Pt(111) surface.

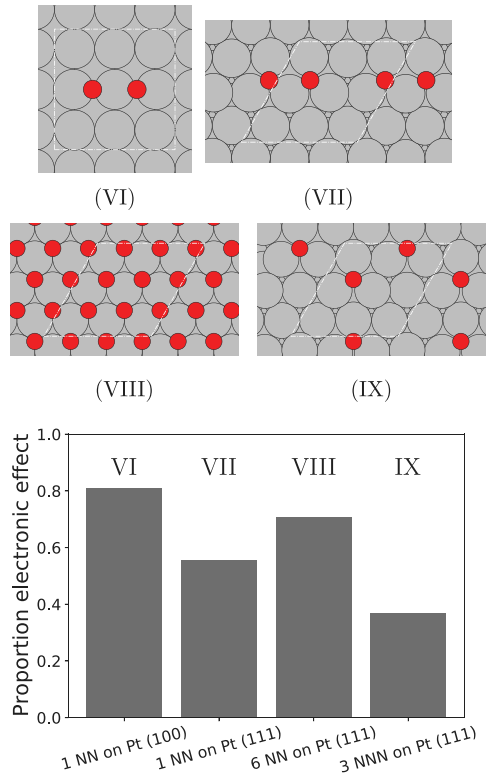

Fig. 3. The fraction of the electronic effects for the AAIs is analyzed for four structures by comparing the interaction energies using a fixed and relaxed surface, respectively.

dominate. The slightly negative interaction energy for the side-by-side configuration indicates that surface distortions contribute. The effect of the surface distortions on the interaction energy is supported by the results in Fig. 2b. The strain is here defined as the average strain between the surface atoms bonded to the adsorbate ($\Delta d/d_0$), and results are provided for both Pt(100) and Pt(111). (All considered structures are visualized in Table S5 A-U.) In agreement with previous work,[37] there is a linear correlation between the interaction energy and the strain. Configuration V (diagonal) is an outlier, which could be explained by a stronger direct electrostatic interaction, due to the short O–O distance or by a stronger surface mediated electronic interaction.

The results in Fig. 2b indicate a correlation between interaction energy and local surface strain. However, the correlation could be indirect and originate from other effects such as differences in coverage and/or surface-mediated electronic effects. Thus, it is important to investigate whether surface-mediated electronic effects also influence the results. To isolate the effects of surface distortions, the interaction energy is calculated with frozen surface atoms. The contribution of electronic effects ($p_{\text{elec.}}$) can in this way be evaluated as:

$$p_{\text{elec.}} = \frac{\Delta E_{\text{ads}}^{\text{fixed}}}{\Delta E_{\text{ads}}^{\text{relaxed}}}, \tag{3}$$

Here, $\Delta E_{\text{ads}}^{\text{fixed}}$ is the interaction energy calculated with a frozen surface, whereas $\Delta E_{\text{ads}}^{\text{relaxed}}$ is the interaction energy when the system is structurally optimized. A large value of $p_{\text{elec.}}$ means that electronic effects dominate the interactions. $p_{\text{elec.}}$ is analyzed for four configurations, Fig. 3. The results show that surface mediated electronic effects dominate the interactions. The surface mediated electronic effects account also for the substantial difference in the interaction energy between the M-connected (I and II) and side-by-side (III and IV) configurations in Fig. 2a. The O adsorbates share a Pt surface atom in the M-connected configuration, which is not the case for the side-by-side configuration. Thus, there is a stronger (positive) interaction in the M-connected case. However, the small negative interaction energy calculated for the side-by-side configuration should be attributed to surface distortions.

To summarize, we have performed a set of DFT calculations to investigate the main contributions for O–O adsorbate–adsorbate interactions

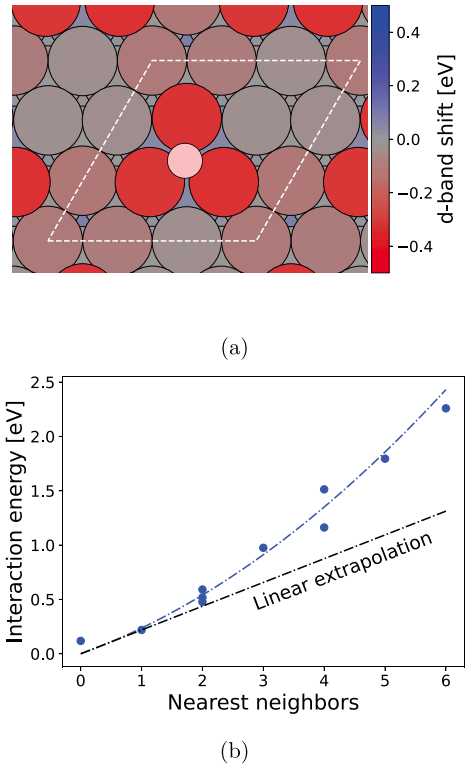

Fig. 4. (a) d-band shifts on the Pt(111) surface owing to an O adsorbate, depicted in pink. (b) Interaction energy of O adsorbates on Pt(111) as a function of the number of nearest neighbors. A linear extrapolation term representing conventional AAI models is shown. The blue line is a guide to the eye. The interaction energy without nearest neighbors is not zero as the structure (Structure B in Table S5) has next nearest neighbors.

on Pt(100). We find that surface-mediated electronic effects dominate the AAI. One way to visualize the surface-mediated interactions is to analyze the O induced d-band shifts, as shown in Fig. 4a. Shifts of the d-band center is often used to quantify changes in the electronic structure [38,39] and known to be a sensitive descriptor for adsorption strength [40]. The local d-band shifts are here computed with respect to a clean surface. The Pt atoms bound to O show the largest shifts, however, the shifts extend over the entire surface cell. The shifts of atoms not directly bound to O are on average 3.7 times smaller than the shifts of the atoms directly bound to O. Thus, the d-band shifts of surface atoms not directly bound to O signals that AAI beyond nearest neighbor effects could be important. This is, furthermore, supported by Fig. 4b, which shows the interaction energies of adsorbed O on Pt(111) (Table S5A-K) as a function of nearest neighbors. It is clear that the adsorbate interactions do not scale linearly with the number of nearest neighbors. Additionally, the differences in interaction energy for configurations with the same number of nearest neighbors again indicates that higher order terms, such as next-nearest-neighbor interactions might be required to obtain an accurate AAI model.

3.2. Model for surface-mediated adsorbate–adsorbate interactions

To develop a simple, but still accurate, interaction model for implementation in kMC simulations, we use a formalism that focuses on the surface mediated electronic effects. This means that we are developing the model treating the dominating interaction mechanism with high accuracy. However, surface-mediated interactions are interlinked with effects of surface distortions and direct electrostatic effects. Thus, all types of effects are accounted for when fitting the parameters to DFT calculations.

The starting point of the model is the calculation of an abstract "electronic change" of the surface atoms, α, owing to the adsorbate. The electronic change is a virtual property that represents a change in the electronic structure. Subsequently, the interaction energy for other adsorbates (changes in adsorption energy) can be calculated based on the electronic change of the metal atom. The electronic change of a specific surface atom α_n $\left(\Delta\varepsilon_{\alpha_n}\right)$ can be expressed as:

$$\Delta\varepsilon_{\alpha_n} = \sum_i \frac{N_{\alpha_n}^{\mathrm{X}_i}}{B^{\mathrm{X}_i}} \Delta\varepsilon^{\mathrm{X}_i}. \tag{4}$$

Here, the summation is performed over all different adsorbates x_i, *e.g.* O, OH and O_2 bound to atom α_n. $\Delta\varepsilon^{\mathrm{X}_i}$ is the electronic change of the metal atom induced by the specie X_i, which is scaled by the number of adsorbates x_i connected to the surface atom α_n $(N_{\alpha_n}^{\mathrm{X}_i})$, divided by the number of surface atoms the adsorbate is bound to (B^{X_i}). The interaction energy experienced by an adsorbate x_i $(\Delta E_{\mathrm{ads}}^{\mathrm{X}_i})$ is calculated from the electronic change of the surface atoms it is adsorbed to:

$$\Delta E_{\mathrm{ads}}^{\mathrm{X}_i} = \frac{f^{\mathrm{X}_i}}{B^{\mathrm{X}_i}} \sum_n \Delta\varepsilon_{\alpha_n}, \tag{5}$$

where the summation is performed over all surface atoms to which x_i is adsorbed to (B^{X_i} terms). f^{X_i} quantifies the effect that the electronic change of the metal atom has on the adsorption energy of the specie X_i.

The induced change in energy of adsorbate (a) due to adsorbate (b) must be equal to the induced change in energy of adsorbate (b) due to adsorbate (a). Hence, for the two adsorbates (a) and (b) sharing a set (m) surface atoms:

$$\Delta E_{\mathrm{ads}}^{\mathrm{a}}(\text{due to b}) = \Delta E_{\mathrm{ads}}^{\mathrm{b}}(\text{due to a}) \tag{6}$$

$$\frac{f^{\mathrm{A}}}{B^{\mathrm{a}}} m \frac{1}{B^{\mathrm{b}}} \Delta\varepsilon^{\mathrm{B}} = \frac{f^{\mathrm{B}}}{B^{\mathrm{b}}} m \frac{1}{B^{\mathrm{a}}} \Delta\varepsilon^{\mathrm{A}} \tag{7}$$

$$\frac{f_A}{\Delta\varepsilon^A} = \frac{f_B}{\Delta\varepsilon^B} = \lambda, \tag{8}$$

hence $f^{\mathrm{X}_i} = \lambda\Delta\varepsilon^{\mathrm{X}_i}$, where λ is a constant independent of X_i. The relation can also be deduced from noting that the electronic change of the surface atoms induced by adsorbate x_i is proportional to the effect of an electronic change on adsorbate x_i. The quantitative value of the change in electronic structure due to the adsorbates is not important for the present purpose, as the focus is the interaction energies, and we can, therefore, let $\lambda = 1$ and, thus, $f^{\mathrm{X}_i} = \Delta\varepsilon^{\mathrm{X}_i}$. Here, $\Delta\varepsilon^{\mathrm{X}_i}$ does not describe a physical value, but rather a virtual property with unit $(\mathrm{eV})^{1/2}$. Eq. (5) is in this case expressed as:

$$\Delta E_{\mathrm{ads}}^{\mathrm{x}_i} = \frac{\Delta\varepsilon^{\mathrm{X}_i}}{B^{\mathrm{x}_i}} \sum_n \Delta\varepsilon_{\alpha_n}. \tag{9}$$

This version of the model is a nearest-neighbor (NN) model, where the sum is performed over the nearest neighbor surface atoms n with respect to the adsorbate.[1]

From the analysis of the O-induced d-band shift (Fig. 4a), it is evident that interactions beyond the nearest neighbors are needed. The surface-mediated model can in similarity to conventional models for AAIs account for next-nearest neighbors interactions:

$$\Delta E_{\mathrm{ads}}^{\mathrm{x}_i} = \frac{\Delta\varepsilon^{\mathrm{X}_i}}{B^{\mathrm{x}_i}} \left[\sum_n^{\mathrm{NN}} \Delta\varepsilon_{\alpha_n} + \gamma_1 \sum_m^{\mathrm{NNN}} \Delta\varepsilon_{\alpha_m} \right] \tag{10}$$

Note that the nearest and next-nearest neighbors in this case are determined with respect to the adsorbate. Hence, an adsorbate in a bridge configuration on an fcc(111) surface has two nearest surface atom neighbors and eight next-nearest surface atom neighbors. (Examples of what is defined as NN and NNN surface atoms are given below

[1] Eq. (9) provides a physical explanation for the validity of Berthelot mixing rules [41] where the interaction between different species can be derived from the interaction between identical species $\Delta E_{\mathrm{ads}}(\mathrm{X}_i, \mathrm{X}_j) = \sqrt{\Delta E_{\mathrm{ads}}(\mathrm{X}_i, \mathrm{X}_i) \cdot \Delta E_{\mathrm{ads}}(\mathrm{X}_j, \mathrm{X}_j)}$, which is easy to prove from Eq. (9).

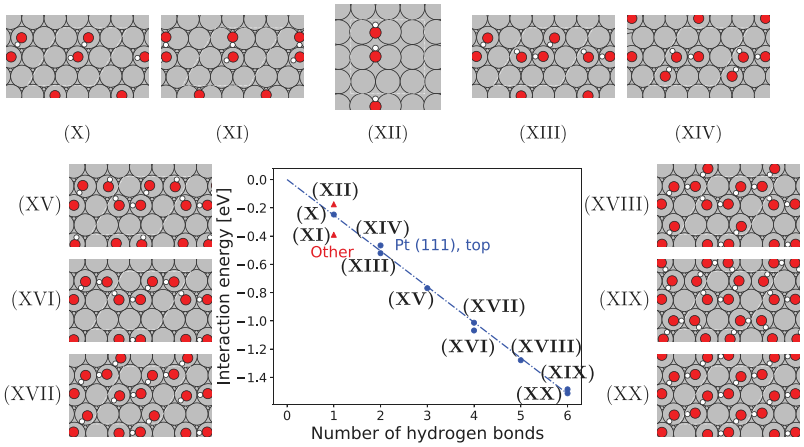

Fig. 5. Hydrogen bonding interaction energy as a function of the number of hydrogen bonds. Atomic color codes: Gray (Pt), red (O), and white (H).

in Fig. 7b.) As the next-nearest neighbor configurations are computationally demanding to determine, and slow down kinetic Monte Carlo simulations, the long-range effects can instead be accounted for using the coverages:

$$\Delta E_{\text{ads}}^{\text{x}_i} = \Delta\varepsilon^{\text{X}_i}\left[\frac{1}{B^{\text{x}_i}}\sum_{n}^{\text{NN}}\Delta\varepsilon_{\alpha_n} + \gamma_2\Delta\varepsilon_{\text{avg}}\right], \tag{11}$$

where γ_2 is a constant, that quantifies the long-range effect of the average electronic structure change $\Delta\varepsilon_{\text{avg}}$ [$(\text{eV})^{1/2}$] on the interaction energy. Note that the γ parameters are optimized in the regression of the model, and differs between the different interaction models. $\Delta\varepsilon_{\text{avg}}$ can be directly related to the coverage as:

$$\begin{aligned}\Delta\varepsilon_{\text{avg}} &= \underbrace{\frac{1}{N_{\text{surf}}}\sum_{n}}_{\text{Site average}}\underbrace{\Delta\varepsilon_{\alpha_n}}_{\text{Eq. (4)}} = \frac{1}{N_{\text{surf}}}\sum_{n}\sum_{j}\frac{N_{\alpha_n}^{\text{x}_j}}{B^{\text{x}_j}}\Delta\varepsilon^{\text{X}_j}\\ &= \sum_{j}\Delta\varepsilon^{\text{X}_j}\underbrace{\frac{1}{N_{\text{surf}}}\sum_{n}\frac{N_{\alpha_n}^{\text{x}_j}}{B^{\text{x}_j}}}_{=\theta^{\text{X}_j}} \qquad (12)\\ &= \sum_{j}\Delta\varepsilon^{\text{X}_j}\theta^{\text{X}_j}, \qquad (13)\end{aligned}$$

where N_{surf} is the number of surface atoms in the system, n runs over all surface atoms, and j runs over all species. In the case of nanoparticles, a variety of surface sites can lead to facet dependent coverages. In such cases, $\Delta\varepsilon_{\text{avg}}$ can be replaced by a sum of the average electronic structure change for a specific type of surface site, weighted by the proportion of neighboring sites of that type. For example, in case the sites are characterized by a generalized coordination number (GCN) [42], the site-specific average electronic shift of adsorbate x_i ($\Delta\varepsilon_{\text{avg}}^{\text{x}_i}$) can be calculated according to:

$$\Delta\varepsilon_{\text{avg}}^{\text{x}_i} = \frac{1}{N_{\text{NNN}}}\sum_{n}^{\text{NNN}}\underbrace{\left[\frac{1}{N_{\text{surf}}^{\text{GCN}_{\alpha_n}}}\sum_{m}^{\text{GCN}_{\alpha_m}=\text{GCN}_{\alpha_n}}\Delta\varepsilon_{\alpha_m}\right]}_{\Delta\varepsilon_{\text{avg},\alpha_n}}, \tag{14}$$

The first summation is performed over the next-nearest neighbors of adsorbate x_i, and the second summation is performed over the surface sites with the same GCN as α_n, giving the average electronic shift of sites with a specific GCN. N_{NNN} is the number of next-nearest neighbors, and $N_{\text{surf}}^{\text{GCN}_{\alpha_i}}$ is the number of surface sites with the same GCN as α_n. After fitting the $\Delta\varepsilon^{\text{X}_i}$ and γ parameters from DFT calculations, the model can be used in kMC simulations. Note that although the formalism of the model is based on surface mediated electronic effects, the effects of direct electrostatic interactions and surface distortions are included via the fitting of the parameters.

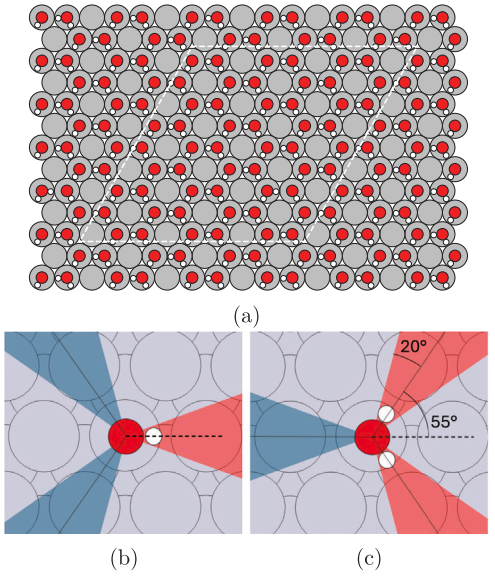

Fig. 6. (a) Optimized OH/H_2O structure by kMC simulations. (b) and (c) Allowed hydrogen bond donating (red) and accepting (blue) directions, for OH and H_2O, respectively. Atomic color codes: Gray (Pt), red (O), and white (H). The dash-dotted line indicates the surface cell.

3.3. Hydrogen bonding interactions

We have up to this point considered non-directional adsorbate–adsorbate interactions. Reactions in aqueous media are often influenced by directional hydrogen bonds. The first step to construct a model for hydrogen bonds is to investigate whether the hydrogen bonds are additive. Fig. 5 shows that the interaction energy between OH adsorbates on Pt(111) is linear with the number of hydrogen bonds, which shows that the hydrogen bonds are additive. Thus, the interaction energies can be extrapolated from the energy of a single hydrogen bond as long as the OH adsorbates are adsorbed at the same surface site (atop).

Based on the calculation of the interaction energy of a single hydrogen bond, we calculate as the next step the hydrogen bond energy for different donor–acceptor couples. Examples of the interactions are given in Table 1. The variation of the hydrogen bond energy is consistent with earlier studies, [43–45] and shows that the interaction energy depends sensitively on the occupation of the oxygen lone electron pair [43].

The strong directionality of hydrogen bonds should be accounted for when including these interactions in kMC simulations. The two

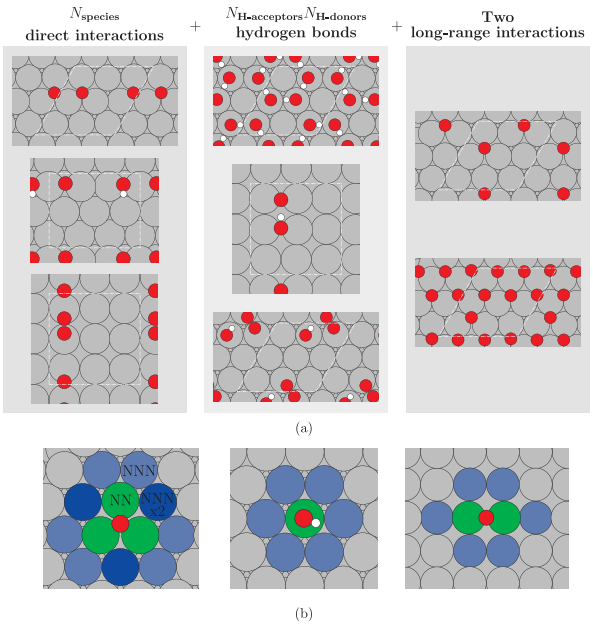

Fig. 7. (a) Suitable structures to fit the surface-mediated NNN and coverage models for a system containing O_2, O, and OH. (b) Visualization of nearest neighbors (NN), in green, and next-nearest neighbors (NNN), in light blue. The dark blue atoms indicate NNN that are double counted as they border two NN surface atoms.

Table 1
Hydrogen bond energy [eV] between different hydrogen donor–acceptor couples.

donor \ acceptor	OH	H_2O	O_2	O
OH	−0.24	−0.15	−0.05	≈0
H_2O	−0.52	−0.17	−0.13	−0.05

hydrogen atoms of a H_2O molecule form an angle of approximately 110°. Thus, an adsorbed water molecule can only form two hydrogen bonds when the acceptors are approximately 110° apart. Similarly, the location of lone pairs constrain the angles at which hydrogen bonds can be accepted. This is illustrated in Fig. 6b–c. Hence, the orientation of OH, H_2O, and other hydrogen bonding adsorbates, needs to be included in kMC simulations. We are here performing kMC simulations starting with 1/3 OH and 1/3 H_2O in random positions. The simulations allow for adsorbate diffusion, rotation and H-transfer from H_2O to OH. The result is shown in Fig. 6a. Owing to the inclusion of the directionality in the hydrogen bonds, the kMC simulations reproduce the long-range order of the half-dissociated water layer, which previously has been reported using X-ray spectroscopy techniques and *ab-initio* molecular dynamics simulations [43,46,47].

3.4. Full AAI model and construction recipe

Combining the surface-mediated NNN and coverage models (Eqs. (10) and (11)) with the hydrogen bonding interactions, the full interaction models can be expressed as:

$$\Delta E^{x_i}_{ads,NNN} = \frac{\Delta\varepsilon^{X_i}}{B^{x_i}}\left[\sum_n^{NN}\Delta\varepsilon_{\alpha_n} + \gamma_3\sum_l^{NNN}\Delta\varepsilon_{\alpha_l}\right] + \sum_m\left[\varepsilon_H^{X_iX_m}\sigma^{x_ix_m} + \varepsilon_H^{X_mX_i}\sigma^{x_mx_i}\right], \quad (15)$$

$$\Delta E^{x_i}_{ads,cov} = \Delta\varepsilon^{X_i}\left[\frac{1}{B^{x_i}}\sum_n^{NN}\Delta\varepsilon_{\alpha_n} + \gamma_4\Delta\varepsilon_{avg}\right] + \sum_m\left[\varepsilon_H^{X_iX_m}\sigma^{x_ix_m} + \varepsilon_H^{X_mX_i}\sigma^{x_mx_i}\right], \quad (16)$$

where n runs over the surface atoms the adsorbate is bonded to (the NN surface atoms, with respect to the adsorbate), l runs over the NNN surface atoms and m runs over the nearest neighbor adsorption sites with respect to the surface atoms (in an aqueous environment, the polar species are located in atop configurations). The definition of NN and NNN surface atoms is visualized in Fig. 7b. $\varepsilon_H^{X_iX_m}$ represents the hydrogen bond energy from specie X_i (donating) towards specie X_m (accepting). $\sigma^{x_ix_m} = 1$ if a hydrogen bond is geometrically allowed from x_i towards x_m, otherwise $\sigma^{x_ix_m} = 0$. The geometric factor is required to describe the directionality of the hydrogen bonds.

Both the surface-mediated NNN and coverage models contain $N_{species} + N_{H\text{-donors}}N_{H\text{-acceptors}} + 1$ parameters, where $N_{species}$, $N_{H\text{-donors}}$ and $N_{H\text{-acceptors}}$ are the total number of species, number of hydrogen donors, and acceptors, respectively. We present here a recipe to obtain a fit from only $N_{species}+N_{H\text{-donors}}N_{H\text{-acceptors}}+2$ data points, thus, including only a single additional degree of freedom. We suggest to include a data point for every adsorbate specie ($N_{species}$), a data point for every hydrogen donor–acceptor pair ($N_{H\text{-donors}}N_{H\text{-acceptors}}$ data points) and two data points to assist fitting the long-range interactions, including one data point with only NNN interactions and one data point with intermediate-high coverage.

For example, a system with O, OH and O_2 adsorbates, requires seven parameters, namely $\Delta\varepsilon^O$, $\Delta\varepsilon^{OH}$, $\Delta\varepsilon^{O_2}$, $\varepsilon_H^{OH\text{–}OH}$, $\varepsilon_H^{OH\text{–}O}$, $\varepsilon_H^{OH\text{–}O_2}$, and $\gamma_{3/4}$. An example of eight appropriate data points used to fit the models are given in Fig. 7a. These structures correspond with the structures B, C, I, AL, AR, AS, AT and AU in Table S5. In case the system also includes H_2O, which is both a hydrogen donor and acceptor, there are six additional parameters, namely $\Delta\varepsilon^{H_2O}$, $\varepsilon_H^{OH\text{–}H_2O}$, $\varepsilon_H^{H_2O\text{–}OH}$, $\varepsilon_H^{H_2O\text{–}O}$, $\varepsilon_H^{H_2O\text{–}O_2}$ and $\varepsilon_H^{H_2O\text{–}H_2O}$.

The model parameters are fitted from interaction energies determined by DFT calculations. Due to the non-linearity of the model, *e.g.* the interaction energy between two O is proportional to $(\Delta\varepsilon^O)^2$, a simple least-squares regression is not possible. Instead, the parameters can be obtained from minimizing the mean squared error of the model:

$$\Delta\varepsilon^O, \Delta\varepsilon^{OH}, \ldots = \arg\min\left\{\sum_i\left[\Delta E^{x_i}_{ads,DFT} - \Delta E^{x_i}_{ads,model}\left(\Delta\varepsilon^O, \Delta\varepsilon^{OH}, \ldots\right)\right]^2\right\}, \quad (17)$$

where $\Delta E^{x_i}_{ads,DFT}$ and $\Delta E^{x_i}_{ads,model}$ are the interaction energies determined from DFT calculations and from the model, respectively. Eq. (17) can be solved by any non-linear optimizer and here the function `scipy.optimize.minimize` from SciPy [48] is employed.

To evaluate the general applicability of the proposed model, the calculations are repeated for Rh, Pd, and Ir. Parameters for the surface-mediated NNN and coverage models are determined from the interaction energies of the structures B, C, I, AL, AR, AS, AT, AU, BB, BC, BD, BF, BG and BK in Table S5. The model is compared with the DFT calculations of all structures with multiple adsorbates in Tables S5–S8 and in the parity plots in Fig. 8. The interaction energy is calculated using Eq. (1). Tables S5–S8 includes the energy of isolated adsorbates and pristine surfaces that are required to calculate the interaction energy of the other structures. Strongly positive interaction energies are present for structures with a high O coverage, whereas strongly negative corresponds to structures with a large number of hydrogen bonds. As expected, the NN model is not sufficient to describe the interaction energy at high coverages, whereas both the surface-mediated NNN and coverage models show good performance. We conclude that as long as the surface distortions are moderate, the surface-mediated NNN and coverage models describe the adsorbate–adsorbate interactions in a sufficient manner. The parameters for the three models are reported in Tables S1–3. The MAE of the models averaged over the four metals is shown in Fig. 8. The MAE per metal is reported in Table S4.

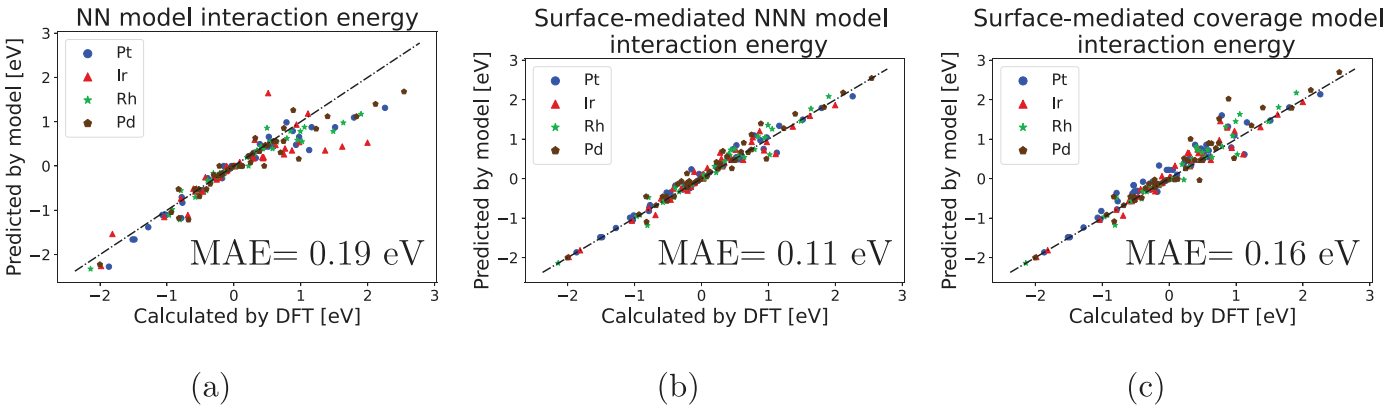

Fig. 8. Parity plot of the AAI models for Pt, Ir, Rh and Pd, including O_2, O, OH, and H_2O. The three models are compared with the DFT calculations. (a) NN, (b) NNN model, and (c) coverage model. The mean absolute error (MAE) is indicated.

4. Conclusions

Using density functional theory calculations we have developed a model for adsorbate–adsorbate interactions between O_2, O, OH and H_2O on Pt, Ir, Rh and Pd surfaces. The model is based on an analysis of the different contributions to the adsorbate–adsorbate interactions, namely (i) direct electrostatic interactions, (ii) indirect surface mediated interactions, (iii) interactions owing to surface distortions, and (iv) hydrogen bonds. We conclude that the main contributions to the adsorbate–adsorbate interactions arise from indirect surface mediated interactions. The model uses a formalism that focus on the indirect surface mediated interactions although all interactions are accounted for via parameter fitting. It is shown that interactions beyond the nearest neighbor interactions are needed to obtain a good agreement with DFT calculations. Two models to include long-ranged interactions are proposed using either the next nearest-neighbor interactions or the effect of the average coverage. Hydrogen bonds are found to be additive and included taking the directionality into account. Our work provides a general framework to understand and parameterize adsorbate–adsorbate interactions. One advantage with respect to conventional AAI models is the small number of calculations and parameters. In the absence of hydrogen-bonds, the presented models contain $N_{\text{species}} + 1$ parameters, while conventional non-directional nearest-neighbor AAI models require $N_{\text{species}}(N_{\text{species}} - 1)/2 + N_{\text{species}}$ parameters. The presented models can be extended to other adsorbates and can efficiently be implemented in kinetic Monte Carlo simulations.

CRediT authorship contribution statement

Willem Vanmoerkerke: Methodology, Investigation, Visualization, Writing – original draft. **Rasmus Svensson:** Supervision, Writing – review and editing. **Henrik Grönbeck:** Conceptualization, Supervision, Funding acquisition, Writing – review and editing.

Declaration of competing interest

The authors declare that they have no known competing financial interests or personal relationships that could have appeared to influence the work reported in this paper.

Acknowledgments

Financial support is acknowledged from the Swedish Research Council (2020–05191). The calculations were performed at NSC via a NAISS grant (2022/3-14). The Competence Centre for Catalysis (KCK) is hosted by Chalmers University of Technology and is financially supported by the Swedish Energy Agency and the member companies Johnson Matthey, Perstorp, Powercell, Preem, Scania CV, Umicore, and Volvo Group.

Appendix A. Supplementary data

Tables with the fitted parameters for the interaction models. Table with MEA for each metal. Table with considered structures and corresponding energies.

Supplementary material related to this article can be found online at https://doi.org/10.1016/j.susc.2024.122678.

Data availability

Data will be made available on request.

References

[1] A.P.J. Jansen, An Introduction To Kinetic Monte Carlo Simulations of Surface Reactions, Vol. 856, Springer, 2012.
[2] R. Svensson, H. Grönbeck, Site communication in direct formation of h2o2 over single-atom pd@au nanoparticles, J. Am. Chem. Soc. 145 (2023) 11579–11588.
[3] Y. Feng, T.V. Janssens, P.N. Vennestrøm, J. Jansson, M. Skoglundh, H. Grönbeck, High-temperature reaction mechanism of nh3-scr over cu-cha: One or two copper ions? J. Phys. Chem. C 128 (2024) 6689–6701.
[4] A.H. Motagamwala, J.A. Dumesic, Microkinetic modeling: a tool for rational catalyst design, Chem. Rev. 121 (2020) 1049–1076.
[5] R.E. Stoller, S.I. Golubov, C. Domain, C. Becquart, Mean field rate theory and object kinetic monte carlo: A comparison of kinetic models, J. Nucl. Mater. 382 (2008) 77–90.
[6] J.B. Benziqer, G.R. Schoofs, Influence of adsorbate interactions on heterogeneous reaction kinetics. formic acid decomposition on nickel, J. Phys. Chem. 88 (1984) 4439–4444.
[7] A. Goswami, H. Ma, W.F. Schneider, Consequences of adsorbate-adsorbate interactions for apparent kinetics of surface catalytic reactions, J. Catal. 405 (2022) 410–418.
[8] A. Bajpai, K. Frey, W.F. Schneider, Comparison of coverage-dependent binding energy models for mean-field microkinetic rate predictions, Langmuir 36 (2019) 465–474.
[9] A. Goswami, W.F. Schneider, Mean field model parameterization to recover coverage-dependent kinetics, J. Catal. 426 (2023) 352–360.

[10] K. Frey, D.J. Schmidt, C. Wolverton, W.F. Schneider, Implications of coverage-dependent o adsorption for catalytic no oxidation on the late transition metals, Catal. Sci. Technol. 4 (2014) 4356–4365.
[11] M. Jørgensen, H. Grönbeck, Montecoffee: A programmable kinetic monte carlo framework, J. Chem. Phys. 149 (2018).
[12] M. Jørgensen, H. Gronbeck, Perspectives on computational catalysis for metal nanoparticles, ACS Catal. 9 (2019) 8872–8881.
[13] L.C. Grabow, B. Hvolbæk, J.K. Nørskov, Understanding trends in catalytic activity: the effect of adsorbate–adsorbate interactions for co oxidation over transition metals, Top. Catal. 53 (2010) 298–310.
[14] A. Kumar, A. Chatterjee, Probabilistic microkinetic modeling: Species balance equations for a catalyst surface containing multiple short-range order parameters to capture spatial correlations, J. Chem. Phys. 160 (2024).
[15] S. Vijay, H.H. Kristoffersen, Y. Katayama, Y. Shao-Horn, I. Chorkendorff, B. Seger, K. Chan, How to extract adsorption energies, adsorbate–adsorbate interaction parameters and saturation coverages from temperature programmed desorption experiments, Phys. Chem. Chem. Phys. 23 (2021) 24396–24402.
[16] E.M. Dietze, H. Grönbeck, Ensemble effects in adsorbate–adsorbate interactions in microkinetic modeling, J. Chem. Theory Comput. 19 (2023) 1044–1049.
[17] P.G. Ghanekar, S. Deshpande, J. Greeley, Adsorbate chemical environment-based machine learning framework for heterogeneous catalysis, Nature Commun. 13 (2022) 5788.
[18] A. Van Bavel, C. Hermse, M. Hopstaken, A. Jansen, J. Lukkien, P. Hilbers, J. Niemantsverdriet, Quantifying lateral adsorbate interactions by kinetic monte-carlo simulations and density-functional theory: No dissociation on rh (100), Phys. Chem. Chem. Phys. 6 (2004) 1830–1836.
[19] N. Lang, S. Holloway, J. Nørskov, Electrostatic adsorbate-adsorbate interactions: The poisoning and promotion of the molecular adsorption reaction, Surf. Sci. 150 (1985) 24–38.
[20] M.J. Hoffmann, A.J. Medford, T. Bligaard, Framework for scalable adsorbate–adsorbate interaction models, J. Phys. Chem. C 120 (2016) 13087–13094.
[21] R. Brako, D. Šokčević, Adsorbate-induced substrate relaxation and the adsorbate–adsorbate interaction, Surf. Sci. 469 (2000) 185–195.
[22] B.W. Chen, S. Bhandari, M. Mavrikakis, Role of hydrogen-bonded bimolecular formic acid–formate complexes for formic acid decomposition on copper: a combined first-principles and microkinetic modeling study, ACS Catal. 11 (2021) 4349–4361.
[23] A. Kulkarni, S. Siahrostami, A. Patel, J.K. Nørskov, Understanding catalytic activity trends in the oxygen reduction reaction, Chem. Rev. 118 (2018) 2302–2312.
[24] G. Kresse, J. Hafner, Ab initio molecular dynamics for liquid metals, Phys. Rev. B 47 (1993) 558.
[25] G. Kresse, J. Hafner, Ab initio molecular dynamics for open-shell transition metals, Phys. Rev. B 48 (1993) 13115.
[26] G. Kresse, J. Hafner, Ab initio molecular-dynamics simulation of the liquid-metal–amorphous-semiconductor transition in germanium, Phys. Rev. B 49 (1994) 14251.
[27] G. Kresse, J. Furthmüller, Efficient iterative schemes for ab initio total-energy calculations using a plane-wave basis set, Phys. Rev. B 54 (1996) 11169.
[28] P.E. Blöchl, Projector augmented-wave method, Phys. Rev. B 50 (1994) 17953.
[29] G. Kresse, D. Joubert, From ultrasoft pseudopotentials to the projector augmented-wave method, Phys. Rev. B 59 (1999) 1758.
[30] J.P. Perdew, K. Burke, M. Ernzerhof, Generalized gradient approximation made simple, Phys. Rev. Lett. 77 (1996) 3865.
[31] S. Grimme, J. Antony, S. Ehrlich, H. Krieg, A consistent and accurate ab initio parametrization of density functional dispersion correction (dft-d) for the 94 elements h-pu, J. Chem. Phys. 132 (2010) 154104.
[32] S. Grimme, S. Ehrlich, L. Goerigk, Effect of the damping function in dispersion corrected density functional theory, J. Comput. Chem. 32 (2011) 1456–1465.
[33] W. Tang, E. Sanville, G. Henkelman, A grid-based bader analysis algorithm without lattice bias, J. Phys.: Condens. Matter. 21 (2009) 084204.
[34] E. Sanville, S.D. Kenny, R. Smith, G. Henkelman, Improved grid-based algorithm for bader charge allocation, J. Comput. Chem. 28 (2007) 899–908.
[35] G. Henkelman, A. Arnaldsson, H. Jónsson, A fast and robust algorithm for bader decomposition of charge density, Comput. Mater. Sci. 36 (2006) 354–360.
[36] M. Yu, D.R. Trinkle, Accurate and efficient algorithm for bader charge integration, J. Chem. Phys. 134 (2011).
[37] M. Mavrikakis, B. Hammer, J. Norskov, Effect of strain on the reactivity of metal surfaces, Phys. Rev. Lett. 81 (1998) 2819–2822.
[38] S.D. Miller, J.R. Kitchin, Relating the coverage dependence of oxygen adsorption on au and pt fcc (1 1 1) surfaces through adsorbate-induced surface electronic structure effects, Surf. Sci. 603 (2009) 794–801.
[39] S.D. Miller, N. Inoğlu, J.R. Kitchin, Configurational correlations in the coverage dependent adsorption energies of oxygen atoms on late transition metal fcc (111) surfaces, J. Chem. Phys. 134 (2011).
[40] J.K. Nørskov, F. Studt, F. Abild-Pedersen, T. Bligaard, Fundamental Concepts in Heterogeneous Catalysis, John Wiley & Sons, 2014.
[41] G.R. Wittreich, S. Liu, P.J. Dauenhauer, D.G. Vlachos, Catalytic resonance of ammonia synthesis by simulated dynamic ruthenium crystal strain, Sci. Adv. 8 (2022) eabl6576.
[42] F. Calle-Vallejo, J. Tymoczko, V. Colic, Q.H. Vu, M.D. Pohl, K. Morgenstern, D. Loffreda, P. Sautet, W. Schuhmann, A.S. Bandarenka, Finding optimal surface sites on heterogeneous catalysts by counting nearest neighbors, Science 350 (2015) 185–189.
[43] T. Schiros, L.-Å Näslund, K. Andersson, J. Gyllenpalm, G. Karlberg, M. Odelius, H. Ogasawara, L.G. Pettersson, A. Nilsson, Structure and bonding of the water-hydroxyl mixed phase on pt (111), J. Phys. Chem. C 111 (2007) 15003–15012.
[44] X.-Z. Li, M.I. Probert, A. Alavi, A. Michaelides, Quantum nature of the proton in water-hydroxyl overlayers on metal surfaces, Phys. Rev. Lett. 104 (2010) 066102.
[45] M. Forster, R. Raval, A. Hodgson, J. Carrasco, A. Michaelides, C (2x 2) water-hydroxyl layer on cu (110): a wetting layer stabilized by bjerrum defects, Phys. Rev. Lett. 106 (2011) 046103.
[46] H. Ogasawara, B. Brena, D. Nordlund, M. Nyberg, A. Pelmenschikov, L. Pettersson, A. Nilsson, Structure and bonding of water on pt (111), Phys. Rev. Lett. 89 (2002) 276102.
[47] V. Tripković, E. Skúlason, S. Siahrostami, J.K. Nørskov, J. Rossmeisl, The oxygen reduction reaction mechanism on pt (1 1 1) from density functional theory calculations, Electrochim. Acta 55 (2010) 7975–7981.
[48] P. Virtanen, R. Gommers, T.E. Oliphant, M. Haberland, T. Reddy, D. Cournapeau, E. Burovski, P. Peterson, W. Weckesser, J. Bright, et al., Scipy 1.0: fundamental algorithms for scientific computing in python, Nat. Methods 17 (2020) 261–272.